

Noisy Simulation of Quantum Beats in Radical Pairs on a Quantum Computer

Brian Rost,^{1,2} Barbara Jones,¹ Mariya Vyushkova,³ Aaila Ali,^{1,4,5}

Charlotte Cullip,^{1,6} Alexander Vyushkov,³ and Jarek Nabrzyski³

¹IBM Research - Almaden, 95120 San Jose, CA

²Department of Physics, Georgetown University, 20057 Washington, DC

³Center for Research Computing, University of Notre Dame, 46556 Notre Dame, IN

⁴Department of Physics, DePaul University, 60614 Chicago, IL

⁵Department of Computer Engineering, Illinois Institute of Technology, 60616 Chicago, IL

⁶Departments of Chemistry and Computer Science, Occidental College, 90041 Los Angeles, CA

(Dated: December 21, 2024)

Current and near term quantum computers (i.e. NISQ devices) are limited in their computational power in part due to imperfect gate operations and imperfect qubits. This naturally constrains the computations run on these devices to be low-depth and short lived, lest the output turn to random noise. Here we seek to take advantage of the imperfect qubit as a means of simulating thermal relaxation in physical systems with no additional computational overhead. As a first step toward this goal we simulate the thermal relaxation of quantum beats in radical pairs on a quantum computer. Our approach is to classically compute a dynamic quantity of interest, construct a parameterized quantum circuit which returns this quantity as a function of the parameters (e.g. magnetic field, time), then simulate the system undergoing thermal relaxation. We simulate the thermal relaxation by 1) explicitly constructing an ancillary circuit to implement Kraus operators associated with the thermal decay channels. 2) Adding wait cycles into the quantum circuit to allow the natural thermal decay of the qubits to effectively simulate the thermal decay of the system of interest. In future work, we hope to remove the classical computation step and directly simulate the time-evolution in parallel with the thermal relaxation. For this paper we chose the Time-Resolved Magnetic Field Effect (TR MFE or MFE) in radical pairs in a magnetic field as the dynamical quantity of interest. This was chosen because it is amenable to analytic solutions classically and also has readily available experimental data, allowing for easy and robust comparison of the results. We find the Kraus operator method gives very accurate results, agreeing with the experiment across its entire range of validity and having a mean squared error of 0.015% compared to the theoretical calculations. We also demonstrate a proof of concept for using the thermal relaxation of the qubits to model the thermal relaxation of the physical system.

I. INTRODUCTION

As spin 1/2 particles like electrons are “nature’s qubits” (simple two-state systems), electron spins map onto quantum devices in a straightforward, natural way. Because of that, it is interesting to focus on quantum applications to chemistry problems involving electron spin dynamics, such as spin chemistry simulations. Spin chemistry is an interdisciplinary subfield of physics and chemistry dealing with magnetic and spin effects in chemical reactions, which connect quantum phenomena like superposition and entanglement directly to macroscopic, measurable chemical parameters such as reaction yields, and make it possible to dynamically visualize those phenomena in chemistry experiments. The key mechanism for magnetic and spin effects in free radical recombination kinetics is the Radical Pair Mechanism (RPM) which, in turn, is based on the principle of total spin conservation in chemical reaction, and singlet-to-triplet time evolution of quantum spin state of a radical pair. Therefore, RPM can be described as time evolution of an entangled state of a two-spin system with magnetic interactions (external magnetic field, or magnetic nuclei present in the radicals), where chemical reaction plays a role of quantum measurement, collapsing the wavefunction into one of the eigenstates (either singlet or triplet). This makes RPM a

good object for quantum simulation.

Among spin chemistry problems, we have identified a simple yet experimentally important model simulation problem - quantum beats in recombination yield of radiation-generated radical-ion pairs¹⁻⁴. Quantum beats are oscillations in singlet-state recombination product yield caused by singlet-to-triplet time evolution of total spin state of a spin-correlated pair of radicals. As spin is conserved in the ionization reaction, the radical pair originating from the same precursor conserves its spin state, which is normally singlet. Therefore, the initial state of the two electron spins in the pair is singlet correlated, or entangled. In the simplest case, with no hyperfine couplings present in both radicals, singlet-triplet oscillations in external magnetic field result from the difference in Larmor precession rates of the two electron spins caused by difference in their g-factors (Fig. 1). The singlet state population in this case is described by the expression¹

$$S_B(t) = \frac{1}{2} \left[1 + \cos((\omega_0 - \omega_1)t) \right] \quad (1)$$

where $S_B(t)$ is singlet state population in magnetic field B , and ω_0 and ω_1 are the Larmor precession frequencies for the two radicals in the pair which depend on B .

In the experiment, a ratio of high-field and low-field recombination kinetics, called the time-resolved magnetic

field effect (TR MFE) is taken in order to get rid of the geminate ion-radical pair recombination kinetics. This quantity is given by¹

$$\text{TR MFE} \equiv M(t) = \frac{I_B(t)}{I_{B_0}(t)} = \frac{4\theta S_B(t) + (1 - \theta)}{4\theta S_{B_0}(t) + (1 - \theta)} \quad (2)$$

where $S_{B_0}(t)$ is singlet state population in low or zero field, and θ is the fraction of singlet-correlated pairs.

Fig. 3 shows the experimental TR MFE curve for a dilute alkane solution containing perdeuterated paraterphenyl (PTP) and perdeuterated diphenylsulphide (DPS) (Fig. 2), in strong magnetic field^{5,6}. In this system, hyperfine couplings are negligible due to the much smaller magnetic moment of deuteron. We were able to map this simulation problem to the IBM Q quantum device and create a quantum circuit (Fig. 4) for IBM Q to reproduce the quantum beats (singlet-triplet oscillations) in this system. In this circuit, each qubit represents an electron spin in a pair.

The qubits are initialized to a singlet state, represented by the Bell state $\Psi^- = (|01\rangle - |10\rangle)/\sqrt{2}$. The Larmor precession of the electron spins is simulated by implementing Z rotations with the rotation angle being proportional to time and precession rate ($R_z(\omega t)$ gates). In order to measure the singlet-state population, we transfer from the total spin state basis to the computational basis with the following transition matrix

$$T = \frac{1}{\sqrt{2}} \begin{pmatrix} \sqrt{2} & 0 & 0 & 0 \\ 0 & 1 & -1 & 0 \\ 0 & 1 & 1 & 0 \\ 0 & 0 & 0 & \sqrt{2} \end{pmatrix} \quad (3)$$

using a gate sequence published in Ref. 7. This implementation is shown in Fig. 4. Since we are only interested in the singlet state population, this circuit can be optimized considerably and the optimized circuit is shown in Fig. 5.

Fig. 6 shows the results of running this circuit shown in Fig. 5 the real 20-qubit IBMQ Almaden⁸ quantum device vs. analytical solution. The observed oscillatory behavior of the singlet state population on the IBMQ device is very close to analytically predicted. To match to experiment, we need to add dissipation, which we will discuss in later sections.

II. QUANTUM BEATS IN 2,2,6,6-TETRAMETHYLPYPERIDINE+./PARATERPHENYL-D14-. RADICAL PAIR (ANALYTICAL SOLUTION)

Now looking at another system, we consider the radical pair 2,2,6,6-tetramethyl-piperidine+.(TMP)/paraterphenyl-d14-.(PTP). As before, this radical pair can be formed by the passage of a burst of radiation through the solution of the two compounds, resulting in ionization of solvent molecules and subsequent capture of electrons by PTP molecules and holes by TMP molecules.

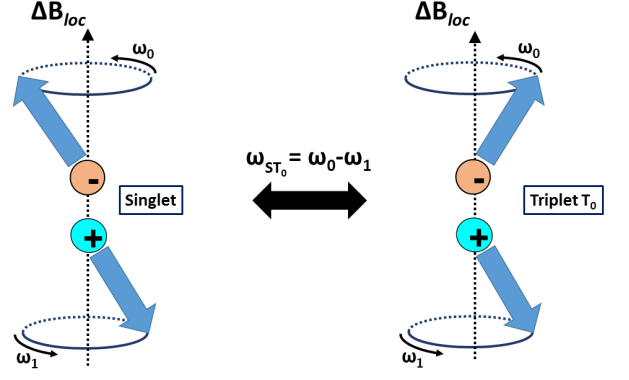


FIG. 1: Vector diagram representing singlet-to-triplet oscillations in a radical pair in strong magnetic field

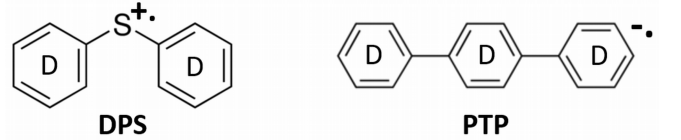


FIG. 2: Structures of DPS and PTP radical ions

The structure of TMP radical appears as in Fig. 7. It is a radical cation, and its unpaired electron spin $\frac{1}{2}$ is localized on the nitrogen atom. There are two magnetic nuclei interacting with electron spin, nitrogen with a nuclear moment of 1, and amine hydrogen with a nuclear moment of $\frac{1}{2}$.

In the deuterated PTP radical, already shown in Fig. 2, unpaired electron spin density is delocalized, and hyperfine couplings are very small due to small magnetic moments of the deuterium nuclei.

The Hamiltonian describing this system is

$$H = \mu_B \mathbf{B} \cdot (g_1 \mathbf{S}_1 + g_2 \mathbf{S}_2) + a_H \mathbf{I}_H \cdot \mathbf{S}_1 + a_N \mathbf{I}_N \cdot \mathbf{S}_1 \quad (4)$$

Here \mathbf{S}_1 and \mathbf{S}_2 refer to the electron spins in TMP and PTP respectively, \mathbf{I}_i refers to the nuclear spin of species i and \mathbf{B} is the magnetic field. The two molecules have different g -factors (g_i), and this gives rise to a quantum beats phenomenon⁹. However, in addition, hyperfine couplings to the nitrogen and hydrogen nuclei on the TMP give rise to the last two terms in the Hamiltonian, with coefficients a_H and a_N . The four interactions in the Hamiltonian affect spin precession, causing mixing between singlet and triplet pairs in this system. The hydrogen and nitrogen HFC constants determined experimentally are $a_H = -1.87\text{mT}$, and $a_N = 1.8\text{mT}$ ⁹.

Diagonalizing the Hamiltonian gives the energies and eignstates of the system, and allows a calculation of the single spin population. The Hamiltonian preserves total spin $\mathbf{S}_1 + \mathbf{S}_2 + \mathbf{I}_H + \mathbf{I}_N$, as well as the z -component of the total spin. With one spin 1 and three spin $1/2$ particles we would have a 24-dimensional matrix to diagonalize, but

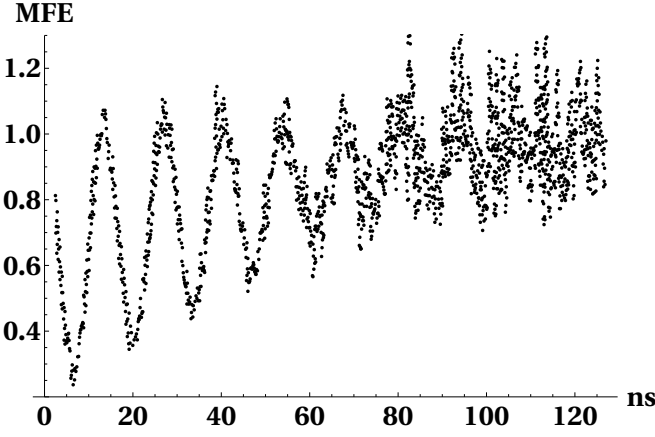


FIG. 3: Experimental time-resolved magnetic field effect for the DPS+./PTP- pair. Data manually pulled from Ref. 6

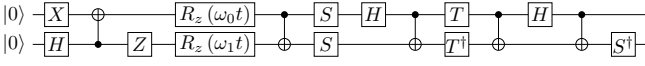


FIG. 4: Quantum circuit for simulation of spin state evolution in a singlet-born radical pair with no hyperfine couplings in both radicals. Singlet state corresponds to measuring $|10\rangle$

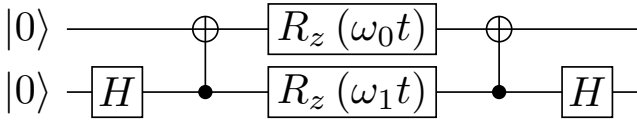


FIG. 5: Optimized, but *not* equivalent to Fig. 4, circuit giving the same singlet probability. Singlet state corresponds to $|00\rangle$

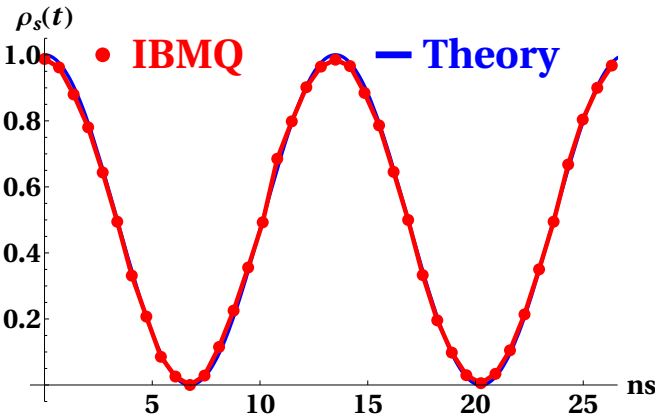


FIG. 6: Simulation of quantum beats in a singlet-born radical pair with no hyperfine couplings, and no paramagnetic relaxation taken into account, on the IBMQ Almaden⁸ quantum device

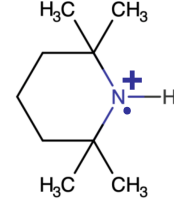


FIG. 7: The radical TMP

forming basis vectors that preserve the spin symmetries causes the 24-dimensional matrix to subdivide into block diagonals of no more than 4×4 , so that all eigenvalues and eigenvectors can be determined analytically.

We show some examples of the rather complex analytical forms for the eigenvectors that result in the appendix, but particularly for $B=0$, the results simplify, and there are only 4 different energies. For the general case of nonzero B , the energies split at large B into three groups, composed of terms of the form $(g_1 + g_2)B$ (large and positive), $(g_1 - g_2)B$ (for the experimental range of B , these terms are of order plus or minus unity), and $-(g_1 + g_2)B$ (large and negative). Using Mathematica, we are able to obtain analytical expressions of eigenvalues and eigenvectors at any value of B .

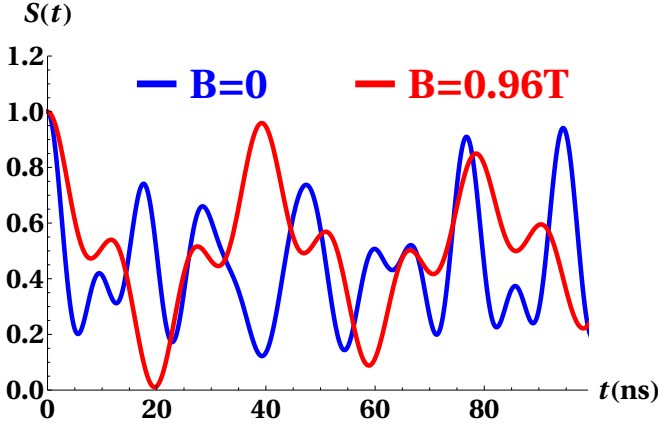
Finally, we form the expression for the expectation of the time evolution of the (total) singlet projection, which we denote as $S(t)$. Fig. 8a shows $S(t)$ at the B values used in experiment (0, 0.96T). These are then combined as per Eq. 2 to yield $M(t)$ or the TR MFE, shown in Fig. 8b. This is the quantity that we will want to use a quantum computer to simulate undergoing thermal relaxation and compare with theory, the quantum simulator, and with experiment.

III. THERMAL DECAY ON A QUANTUM COMPUTER

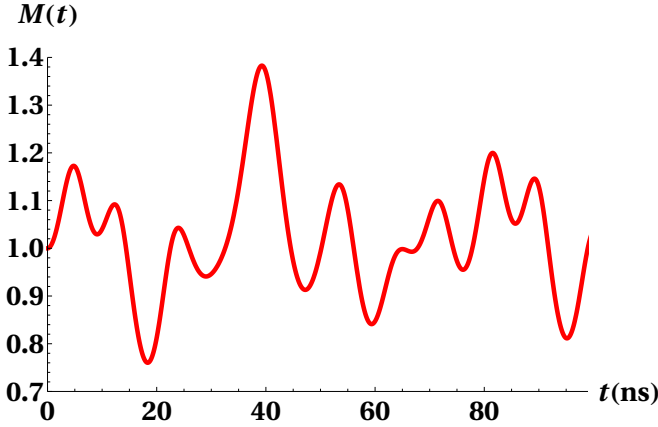
Our goal is to reproduce the thermal relaxation seen in experiments using a quantum computer. We do this first using the simulator Qiskit, and then go on to use the quantum hardware, and these approaches will be described in this order.

The first challenge in using the simulator Qiskit and AER to simulate the noise was determining among the many different kinds of noise, including noise on the gates and on the qubits, which was the best to compare to experiment. We tried this first for the DPS-PTP pair of Section II, where the experimental results are very clear, and where there are fewer oscillatory frequencies to compare to.

After trying combinations of several different types of error, singly in and sets, we found that to compare best to the experiment, only one type of error was needed to be added, and that was thermal noise applied to the $R_z(\omega t)$ gate acting on each qubit. Applying the error to the measurement operation, as well as applying the $R_z(\omega t)$ gate



(a) Plot of $S(t)$ for $B = 0$ and large $B = 0.96T$ corresponding to the fields used in experiment. They still have oscillatory behavior as seen in Fig. 6 but with added structure due to hyperfine interactions.



(b) Plot of theoretical prediction for $M(t)$ without any thermal relaxation.

FIG. 8: Theoretical calculation of the quantities of interest without any thermal relaxation.

to just one qubit, gave physically unreasonable results.

In the theory of quantum beats, paramagnetic relaxation in a radical pair in strong magnetic field is described by two decay rate parameters: longitudinal relaxation time T_1 and transverse relaxation (dephasing) time T_2 . The singlet state population with paramagnetic relaxation effects taken into account, with some minor approximation (see next section), is given by the expression

$$S_B(t) = \frac{1}{4} + \frac{1}{4}e^{-t/T_1} + e^{-t/T_2} \left(\bar{S}_B(t) - \frac{1}{2} \right) \quad (5)$$

where $\bar{S}_B(t)$ is the singlet state population calculated ignoring paramagnetic relaxation¹.

For the DPS/PTP pair, the experimentally determined relaxation rate parameters are: $T_1(DPS) = T_2(DPS) = 50\text{ns}$; $T_1, T_2(PTP) \gg T_1, T_2(DPS)$ ⁶. Relaxation rates

Experimental Parameters		
Parameter	Low B	High B
B	0.017T	0.96T
ω	$4.8 \times 10^8 \text{s}^{-1}$	$8.1 \times 10^6 \text{s}^{-1}$
p	0.499	0.500

TABLE I: Experimental parameters for DPS/PTP radical pair. Here B is the magnetic field strength. ω is the difference in Larmor precession frequencies of the two radicals and $p = (1 + e^{g\mu_B B\beta})^{-1}$ is the equilibrium population of the upper Zeeman sublevel. For both field strengths, the fraction of singlet correlated pairs is $\theta = 0.47$

for the radical pair are related by

$$\frac{1}{T_{1,2}} = \frac{1}{T_{1,2}(DPS)} + \frac{1}{T_{1,2}(PTP)} \approx \frac{1}{T_{1,2}(DPS)}. \quad (6)$$

To generate the relaxation noise, we used a modification of Qiskit AER's "thermal relaxation error" module to run the circuit shown in Fig. 4. In addition to the relaxation rate parameters, we introduced the dephasing error caused by hyperfine couplings in the PTP radical anion. Unlike the exact treatment of hyperfine coupling of the previous section, here we approximate the hyperfine structure of the PTP radical anion as a Gaussian distribution of hyperfine components¹⁰. In this case, the expression Eq. 2 for TR MFE becomes⁶:

$$M(t) = \frac{1 + \theta e^{-t/T_1} + 2\theta e^{-[t/T_2 + \sigma^2 t^2/2]} \cos(\omega_0 t)}{1 + \theta e^{-t/T_1} + 2\theta e^{-[t/T_2 + \sigma^2 t^2/2]} \cos(\omega_1 t)} \quad (7)$$

Where¹⁰ $\sigma_a = \sqrt{\frac{1}{3} \sum_n a_n^2 I_n(I_n + 1)}$ is the second moment of the Gaussian distribution of the hyperfine components. Based on the hyperfine coupling constants reported in¹¹, $\sigma = 1.45 \times 10^7 \text{s}^{-1}$ for the PTP radical anion.

Note that a new term, quadratic in time, has appeared in the dephasing exponent. We modified the standard Qiskit AER thermal relaxation error module by adding this quadratic term to dephasing error, with σ as a parameter. Fig. 9 shows the simulation results where the modified thermal relaxation error was applied to the circuit shown in Fig. 4, and the TR MFE ratio was taken according to Eq.7, compared to the experimental data. The experimental parameters used for high-field and low-field simulations are listed in Table I. The simulation shows very good agreement to the experiment; the oscillation frequency, the decay rate, and the general upward drift of the TR MFE curve are reproduced extremely well.

For TMP/PTP, the circuit used is analogous to that shown in Fig. 5 but the rotations are modified because the hyperfine couplings give rise to many frequencies and the phase no longer precesses at a constant rate. Thus we can no longer simply rotate each qubit by the respective

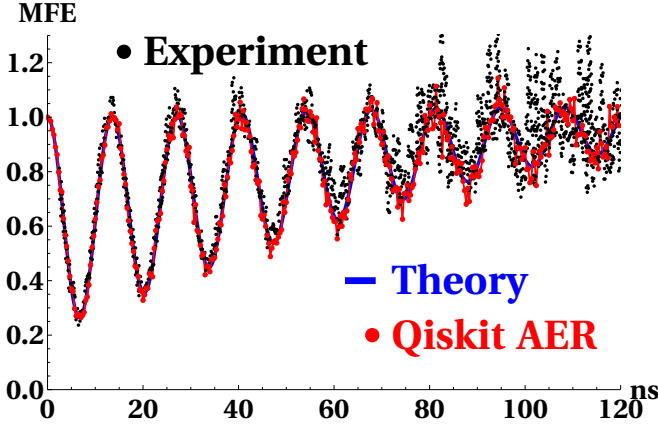


FIG. 9: Comparison of theory, Simulator with AER, and experiment for DPS/PTP radical pair. Note improved fit to data with use of noise on the Simulator.

frequency. Instead we simply rotate one qubit by the precomputed time dependent value.

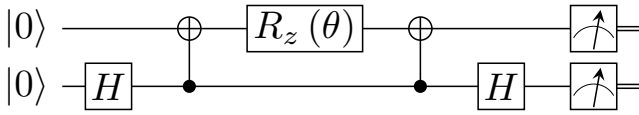


FIG. 10: Raw circuit returning the probability of the TMP/PTP radical pair being in a singlet state over time, $S(t)$, as the probability of measuring 00. This quantity is explicitly encoded in $\theta = 2 \cos^{-1}(\sqrt{S(t)})$.

We present two approaches to simulating the thermal

relaxation and discuss advantages and disadvantages of each. 1) We explicitly simulate the amplitude damping and dephasing channels using ancilla qubits. This has the advantage of being highly controllable in that we are free to construct thermal decay with any parameters we wish. However, it has the disadvantage of requiring a larger and deeper circuit which makes it less reliable on NISQ devices. 2) We leverage the thermal decay of the qubits themselves to model the thermal decay of the radical pair system. This has the advantage that the circuit remains small and simple. But has the disadvantage that we are not in control of the decay parameters. An in-depth discussion is given below.

The main mechanisms of relaxation in the system are amplitude damping (T_1) and dephasing (T_2)⁶. The TR MFE, our quantity of interest, is a ratio involving the singlet population in time for high magnetic field to zero magnetic field. For the TMP/PTP radical pair we have: $T_1 \gg T_2$ for large B while $\tau \equiv T_1 = T_2$ for $B = 0$ ⁶. From these considerations it is straightforward to derive an expression for the evolution of the singlet state probability, $\tilde{S}(t)$, of the damped system, in terms of the singlet state probability for the isolated system, $S(t)$, as shown in Eq. 8. For this work we will precompute $S(t)$. Both $S(t)$ and $\tilde{S}(t)$ can be found by direct matrix multiplication of the circuit in Fig. 10 and by applying the Kraus operators representing the dephasing and amplitude damping channels (more details given Section III A). As quantum hardware continues to improve, it would be interesting to attempt to simulate the Hamiltonian dynamics to get $S(t)$ directly from the quantum computer in addition to simulating the thermal relaxation of the system.

$$\tilde{S}(t) = \frac{1}{2} \left(e^{-t/T_2} (2S(t) - 1) - e^{-t/(2T_1)} (n - \bar{n})^2 - (2n\bar{n} - 1) (e^{-t/T_1} + 1) \right) \quad (8)$$

Here $n = (1 + e^{-\beta})^{-1}$ is the Fermi function which gives the equilibrium population of the ground state as a function of inverse temperature, β , measured in units of the energy of the excited state. $\bar{n} = 1 - n$ is the equilibrium population of the excited state.

To a very good approximation, our system is at the infinite temperature limit. The Zeeman level splitting is over 2 orders of magnitude smaller than room temperature thermal energy. This reduces Eq. 8 to

$$\tilde{S}(t) = \frac{1}{4} \left(1 + e^{-t/T_1} + e^{-t/T_2} (4S(t) - 2) \right) \quad (9)$$

which further gives

$$\tilde{S}_B(t) = \frac{1}{2} \left(1 + e^{-t/T_2} (2S(t) - 1) \right) \quad (10)$$

$$\tilde{S}_0(t) = \frac{1}{4} \left(1 + e^{-t/\tau} (4S(t) - 1) \right) \quad (11)$$

So finally the quantity we are trying to match is given by

$$\tilde{M}(t) = \frac{4\theta\tilde{S}_B(t) + (1 - \theta)}{4\theta\tilde{S}_{B_0}(t) + (1 - \theta)} \quad (12)$$

In in Fig. 11 we plot $\tilde{M}(t)$ from Eq. 12 as a function of time, compared to experiment^{9,12,13} on the TMP/PTP radical pair. The discrepancy between theory and experiment at $t < 10$ ns is due to additional short-lived, non-magnetosensitive fluorescence observed in the experiment. This fluorescence comes from excited TMP and

PTP molecules formed by energy transfer from singlet-excited solvent molecules.⁹

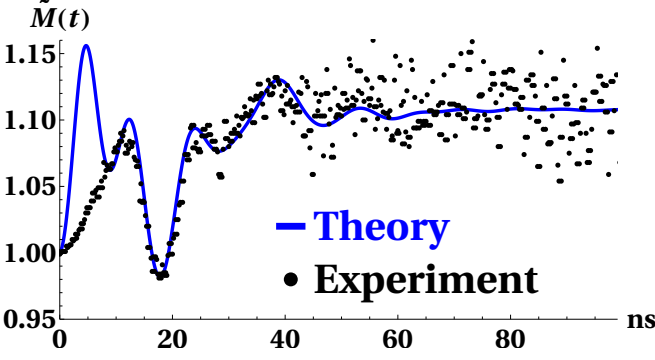


FIG. 11: Comparison of $\tilde{M}(t)$ from Eq. 12 at infinite temperature ($\beta \rightarrow 0$) with experimental data⁹ on the TMP/PTP radical pair.

A. Explicit Decay

One way to model the thermal decay of our system is to explicitly simulate the noise channels acting on our system using ancilla qubits. The main mechanisms of qubit decay are amplitude damping (T_1) and dephasing (T_2).

The TR MFE, our quantity of interest, is a ratio involving the singlet population in time for high magnetic field to zero magnetic field. For the TMP/PTP radical pair we have: $T_1 \gg T_2$ for large B while $T_1 = T_2$ for $B = 0$ ⁶.

The Kraus operators associated with amplitude damping at zero temperature are given by¹⁴

$$K_0 = \begin{pmatrix} 1 & 0 \\ 0 & \sqrt{1-p_x} \end{pmatrix} \quad K_1 = \begin{pmatrix} 0 & \sqrt{p_x} \\ 0 & 0 \end{pmatrix} \quad (13)$$

Where p_x is the probability of a qubit in state $|1\rangle$ to decay to state $|0\rangle$. Iteratively applying this channel and taking the characteristic decay time of the qubit to be T_1 , we find that solving for p_x gives the well known result that

$$p_x = 1 - e^{-t/T_1}. \quad (14)$$

This gives a nice simplification for large B , where $T_1 \gg T_2$ so we may take $T_1 \rightarrow \infty$. This gives $p_x^B = 0$ and we may neglect the amplitude damping channel altogether. For $B = 0$ we must simulate both channels.

The dephasing channel is given by

$$K_0 = \sqrt{1-p_z}I \quad K_1 = \sqrt{p_z}Z \quad (15)$$

We would like to be able to set the dephasing rate, T_2 . Since the amplitude damping channel itself performs dephasing with a decay constant of $2T_1$ we must consider the action of both the channels together. It is straightforward to work out that to achieve a dephasing time of

T_2 , one must choose $p_z = (1 - e^{-t/(2/T_2 - 1/T_1)})/2$. For high B , we take the limit $T_1 \rightarrow \infty$ while for $B = 0$ we take $\tau \equiv T_1 = T_2$ which gives

$$p_z^B = \frac{1}{2} (1 - e^{-t/T_2}) \quad p_z^0 = \frac{1}{2} (1 - e^{-t/(2\tau)}) \quad (16)$$

It is important to note that we wish to simulate a system at room temperature, which has fundamentally different behavior than the zero temperature behavior. The proper finite temperature amplitude damping channel requires two additional Kraus operators to simulate excitation from $|0\rangle$ to $|1\rangle$. However for our specific situation, it turns out that this is not necessary, due to the symmetry in the singlet state. We find that applying the zero temperature decay channel to a single qubit gives identical results as applying the infinite temperature channel to both qubits, except the decay is slowed by a factor of two. Given the energy scales in our system, the infinite temperature approximation is a very good one; this allows us to save computational resources in simulating the infinite temperature 2-qubit system by applying the zero-temperature channel to only one of them.

Armed with Kraus operators it is easy to create a circuit that implements them following the approaches given in 15 and 16. Intuitively, it is useful to think of the amplitude damping channel as being “If the qubit is in $|1\rangle$, apply an X gate with probability p_x . Otherwise do nothing”, and the dephasing channel being “With probability p_z apply a Z gate”. In this way it is easy to make sense of the circuit given in Fig. 12.

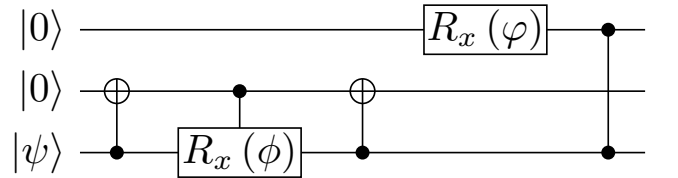


FIG. 12: Circuit to amplitude damp and dephase a qubit. First three gates accomplish the amplitude damping while the final two implement the dephasing

The first 3 gates implement amplitude damping by first mapping the state of the system qubit onto an ancilla with a cX gate. Then, if the system qubit is in $|1\rangle$, so is the ancilla and the cRx rotates the system from $|1\rangle$ toward $|0\rangle$. It is easy to show that one must choose $\phi = 2\sin^{-1}(\sqrt{p_x}) = 2\cos^{-1}(e^{-t/(2T_1)})$ to give the proper probability of decay.

Similarly the final 2 gates implement dephasing by a similar trick. We rotate an ancilla so it has probability p_z of being in $|1\rangle$ then applying a Z gate controlled on this ancilla. Again it is easy to work out that $\varphi = \cos^{-1}(1 - 2p_z)$ gives the proper probability of dephasing.

The dephasing may be simplified by noting that the controlled Z is there to implement a \tilde{Z} with probability p_z . We can do this manually by simply splitting the runs into a batch with a Z gate and a batch without. Then

taking the average of the results, weighted by $w_z = p_z$ and $1 - w_z$ respectively, gives the same result as before. This approach is preferable because (after transpilation to IBM's native gate set) it uses one fewer qubits, two fewer U_3 gates and one fewer cX gates. This results in much better fidelity. Putting this altogether gives the final circuits as shown in Fig. 13.

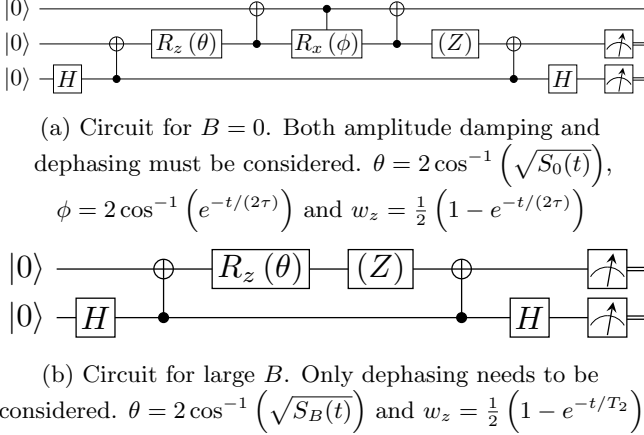


FIG. 13: Circuits to simulate the thermal relaxation of our system. The singlet state corresponds to measuring $|00\rangle$. (Z) indicates that the shots are to be split between implementing the circuit including the Z gate and omitting the Z gate. Results are then combined as $S = w_z P_{00}^Z + (1 - w_z) P_{00}^{no Z}$

We confirm the correctness of the method by direct matrix multiplication of the circuit and verify the results match the theory exactly. We test the feasibility of the method by first simulating the action of the circuits in Qiskit¹⁷ using 5,000 shots - just like we would on the actual hardware. The results match the theory extremely well, as shown in Fig. 14, giving confidence that the method is usable even with noisy counting statistics.

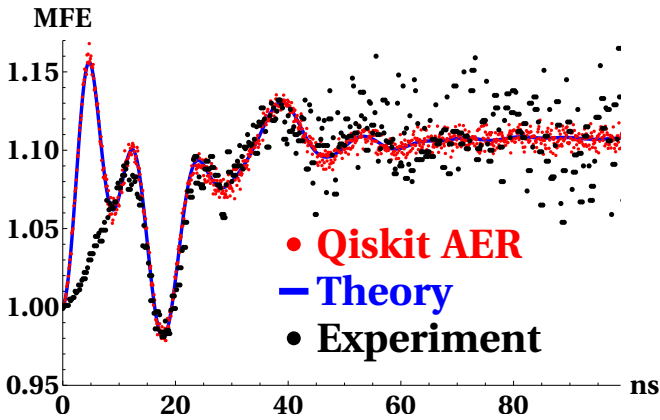


FIG. 14: Results of simulating the circuits shown in Fig. 13 using Qiskit with 10^5 shots each, then recombining via Eq. 2 to produce $\tilde{M}(t)$. The match is essentially perfect.

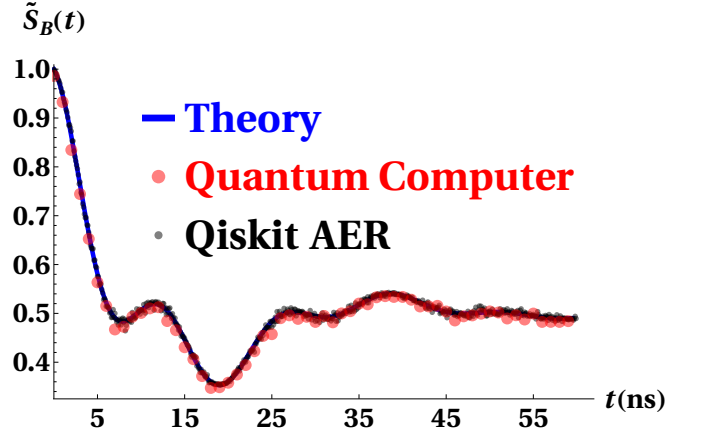


FIG. 15: Results of running the circuit from Fig. 13b on the IBMQ Almaden quantum device vs. simulating the circuit in AER vs. the calculated $\tilde{S}_B(t)$ in Eq. 10. The results are highly accurate with a mean squared error of 0.011%.

Running the circuits shown in Fig. 13 on the actual hardware introduces error associated with imperfect gates, qubits and measurements. Thus care was taken to select the optimal qubits to minimize the error incurred by the cX and rotation gates, while Qiskit Ignis' measurement error mitigation protocol was used to correct for measurement errors¹⁷.

The results for simulating large B using the circuit in Fig. 13b are shown in Fig. 15 and are excellent despite the potential errors incurred by using a NISQ device. Note that the R_z and Z gates are implemented as frame shifts on IBM's hardware and are thus exact operations, so the high B circuit is quite simple.

We find that simulating $B = 0$ (circuit in Fig. 13a) is more error prone and the results are shown in Fig. 16. This is unsurprising since the $B = 0$ circuit requires the addition of an ancilla qubit, four cX gates and two U_3 gates. Again Qiskit Ignis' measurement error mitigation protocol was used to correct for measurement errors¹⁷. The mean squared error for the $B = 0$ runs was 8.5 times higher than the large B runs, at 0.097%. However, this is still quite good.

Putting this two results together allows us to calculate the target quantity, $\tilde{M}(t)$, and compare against experiment. This is shown in Fig. 21 together with the results from using the inherent qubit noise to model the thermal decay. Overall the Kraus operator protocol described in this section gives high quality results that agree with experiment to a good degree across the entire range of validity of the experiment.

B. Leveraging Inherent Qubit Noise

An entirely different approach to simulating the thermal relaxation of a system is to try to take advantage of the

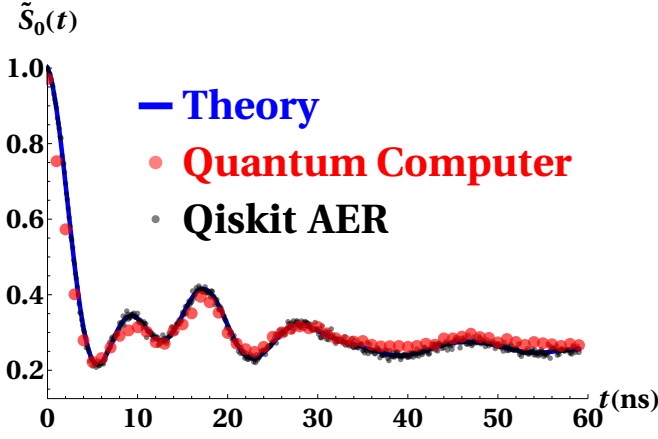


FIG. 16: Results of running the circuit from Fig. 13a IBMQ Almaden quantum device vs. simulating the circuit in AER vs. the calculated $\tilde{S}_0(t)$ in Eq. 11. The results are quite accurate with a mean squared error of 0.096%.

inherent thermal relaxation of the qubits in the quantum computer. This approach is appealing in that it does not rely on explicitly simulating dissipative channels; this will become increasingly expensive in time and space as system sizes grow. This is particularly advantageous for the amplitude damping, since dephasing can be implemented practically for free. It is also an interesting application of NISQ devices, whose noise often hinders quantum simulation. Here we hope to turn that around and use the noise as an integral part of the simulation.

This approach has many challenges. Firstly, for the large B case we have that $T_1 \gg T_2$. This is not compatible with the natural behavior of qubits. Because of this, and since dephasing is essentially free to implement, we focus on the case of $B = 0$, implemented by the circuit shown in Fig. 10. Here we have $T_1 = T_2$ which is reasonable for qubits. However, the time to implement the gate sequence of the circuit is typically around 3 to 4 orders of magnitude shorter than that of the decay time of the qubits. Furthermore the time to implement the sequences is constant while we need the duration to increase with simulated time. This can be overcome easily by adding wait cycles into the circuit by using identity gates. We choose the number of identity gates to use as

$$n_{id} = \frac{t T_{qu}}{T_{rp} t_{id}} \quad (17)$$

Where t is the simulated time, T_{qu} is the average of T_1 and T_2 over both qubits, T_{rp} is the decay time of the radical pairs and t_{id} is the duration of the wait cycle implemented by the identity gate. T_{qu} and t_{id} are provided by the backend in Qiskit.

Another challenge is that the qubits are effectively in a 0 temperature environment while the radical ion solution is effectively in an infinite temperature environment. This will strongly affect the resulting dynamics and must be

corrected for.

To do the correction we measure the decay of a state which is constant in time and use that data to correct the results from the 0 temperature qubits back to any target temperature. Denote the quantity $S'(t)$ as the probability of measuring $|00\rangle$ after preparing a Bell state as per the circuit in Fig. 17. Note that this is the same as measuring the circuit in Fig. 10 before transforming to the Bell basis as the R_z gate does not alter the population of $|00\rangle$. Then the temperature corrected result is given by, in intuitive form

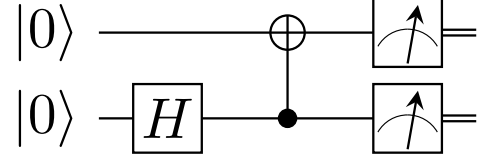


FIG. 17: Circuit to perform temperature correction

$$\tilde{S}^\beta(t) = \underbrace{\tilde{S}^0(t)}_{\text{Raw}} - 2 \underbrace{(\tilde{S}^0(\infty) - \tilde{S}^\beta(\infty))}_{\text{Temperature Weight}} \underbrace{(S'(t) - S'(0))}_{\text{Time Weight}} \quad (18)$$

The temperature weight can be thought of as the long time limit singlet population difference between the qubits and the radical pairs. The time weight can be thought of as a measure of how far along the decay is. For actually computing this reduces to

$$\tilde{S}^\beta(t) = \tilde{S}^0(t) - n\bar{n} (2S'(t) - 1) \quad (19)$$

And in our specific case of infinite temperature, $n = 1/2$ and so

$$\tilde{S}(t) = \tilde{S}^0(t) - \frac{1}{4} (2S'(t) - 1) \quad (20)$$

As a check, we can explicitly compute the exact $S'(t)$ by directly applying the amplitude damping and dephasing channels to the final state before measurement. Doing this we find

$$S'(t) = \frac{1}{2} \left(e^{-t/T_1} - 2e^{-t/(2T_1)} + 2 \right) \quad (21)$$

Eq. 8 gives the time dynamics of the system with arbitrary temperature. In the infinite temperature limit we have $n = 1/2$ which reduces 8 to

$$\tilde{S}^\infty(t) = \frac{1}{4} \left(1 + e^{-t/T_1} + e^{-t/T_2} (4S(t) - 2) \right) \quad (22)$$

In the 0 temperature limit $n = 1$ so

$$\tilde{S}^0(t) = \frac{1}{2} \left(1 - e^{-\frac{t}{2T_1}} + e^{-\frac{t}{T_1}} + e^{-\frac{t}{T_2}} (2S(t) - 1) \right) \quad (23)$$

It is indeed the case that

$$\tilde{S}^0(t) - \frac{1}{4}(2S'(t) - 1) = \tilde{S}^\infty(t) \quad (24)$$

As a proof of concept we simulate the circuit shown in 10, with thermal noise added to the qubits using Qiskit AER's "thermal relaxation error" noise model. Qiskit takes as input the qubits temperature (0), time, T_1 and T_2 and then simulates the circuit assuming the qubits thermally relax following amplitude damping and dephasing. The results are shown in Fig. 18 and have excellent agreement with the theory.

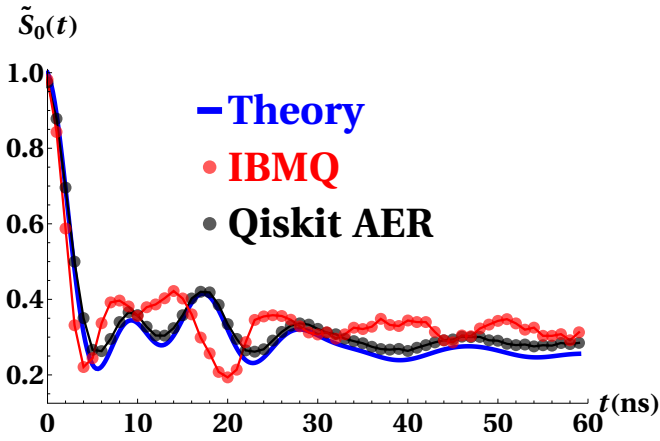


FIG. 18: Comparison of theoretical thermal relaxation vs. AER simulation results using the Almaden backend error model vs. running the circuit shown in Fig. 10 on the IBMQ Almaden quantum device

When we run this protocol on actual quantum hardware, a strange effect arises. As can be seen in Fig. 18 the time axis appears to have been compressed by a factor of about 0.85. This is quite interesting as we explicitly put $S(t)$ into the protocol and neither amplitude damping nor dephasing could shift the location of the peaks.

More evidence for an extra noise source is found when we examine the behavior of $S'(t)$ as shown in Fig. 20. Some sort of oscillatory behavior is observed when the circuit for this (shown in Fig. 17) is completely constant in time. More study is needed to identify and characterize this source of noise. It is not entirely unexpected that things become slightly unstable when forcing runs to go on for 10s to 100s of μ s.

We can reconstruct $\tilde{M}(t)$ from the previously obtained large B data and the $B = 0$ data shown in Fig. 19. The result is shown in Fig. 21. Despite the heavy noise levels in the $B = 0$ data (MSE of 18%), the reconstructed $\tilde{M}(t)$ is fairly accurate (MSE of 4.4%).

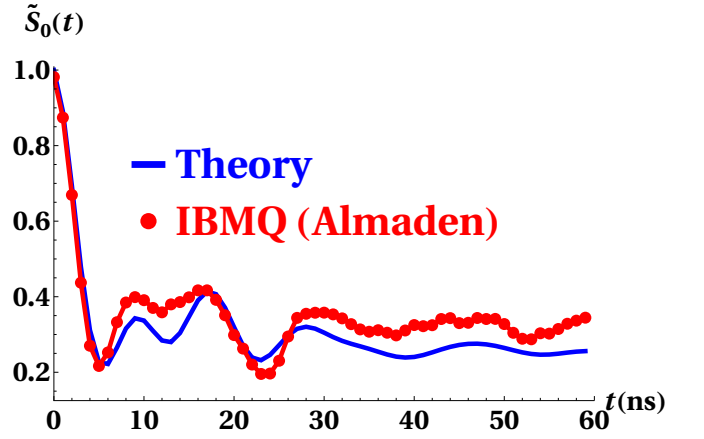


FIG. 19: Stretching the results out gives by the right general shape, although the noise is considerable.

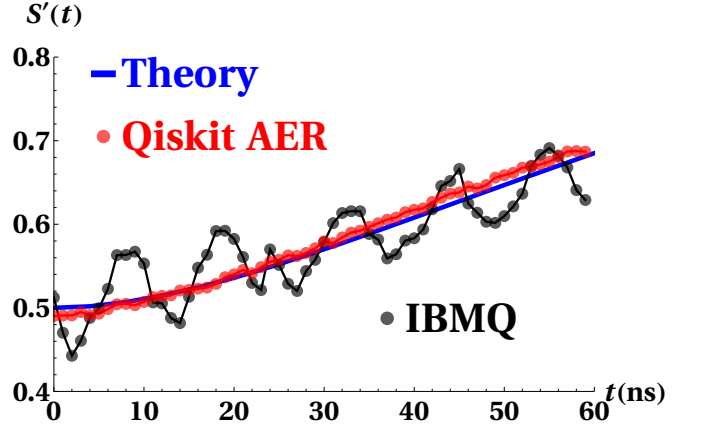


FIG. 20: Comparison of theoretical calculation of $S'(t)$ vs. result of simulating the circuit from Fig. 17 using device noise model in AER vs. the result of running the circuit from Fig. 17 on the IBMQ Almaden quantum device. The data from the actual device shows the existence of a quasi-periodic noise signal that is unknown to AER.

IV. CONCLUSION

We have shown that thermal relaxation may be simulated effectively on a quantum computer with minimal added resources. Dephasing may be done for free by splitting the allocated shots between the bare circuit and a circuit with a Z gate added to a qubit. To dephase multiple qubits becomes more complicated as treating the probabilities of dephasing properly becomes a combinatorial problem in selecting to which subsets of qubits to apply a Z gate. However this can be overcome by applying R_z gates to every qubit, with the angles drawn from a normal distribution of mean 0 and variance $4t/T_2$. In this way there is no extra quantum cost and minimal extra

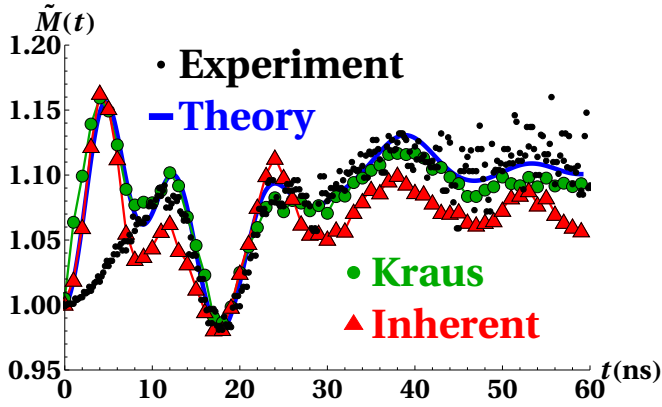


FIG. 21: Reconstructed $\tilde{M}(t)$ from the results shown in Figs. 15,16 and 15,19. The results using the Kraus method are highly accurate with a mean squared error of 0.015%, agreeing with the experimental data across all times within the experimental range of validity. The results using the inherent noise on the qubits produced less accurate results (MSE of 4.4% compared to theory) and required stretching the data after the fact.

classical cost to dephasing an arbitrarily large system of qubits.

Amplitude damping on the other hand is more difficult as it is applied conditionally depending on the state of a qubit. This requires mapping this system state onto an ancilla, rotating the system state conditioned on this ancilla, then undoing the mapping. Thus performing amplitude damping on a system of N qubits incurs an extra cost of N ancilla qubits, $4N$ cX gates and $2N$ U_3 gates. Double all of these figures to perform arbitrary amplitude damping at finite temperature to simulate excitation in addition to decay. This may become prohibitive in this NISQ era where connectivity is limited and it is critical to keep circuit depth short while minimizing 2-qubit operations. However the cost scales only linearly in size and depth so such an approach is certainly a benefit over classical simulation at scale.

We demonstrate the effectiveness of these techniques on a simple system of two entangled qubits undergoing thermal relaxation. This system is simple enough to allow for an exact classical solution while still showing non-trivial relaxation behavior. Furthermore this system is of interest in quantum chemistry and so we may compare

our simulation results to actual experimental data. We find excellent agreement between theory, experiment and our dissipative quantum simulations. This shows that such a method is an effective tool to model real world systems undergoing thermal relaxation that is useable on currently available quantum devices. Additionally using this method to add thermal relaxation scales linearly with system size leaving open the possibility of tackling large systems in the near term.

We have also shown the feasibility of performing the thermal decay by utilizing the inherent noise within the quantum computer itself. We have demonstrated, for our specific system, a protocol allowing for the recovery of the relaxation dynamics at arbitrary temperature from the zero temperature relaxation of the qubits. This protocol involves combining the results from two different measurements; one which models the relaxation of the zero temperature system using the qubit relaxation itself, and one which tracks the qubit decay to be used to “undo” some of the decay in a classical post-processing step.

For our small and simple system, this protocol gives considerably lower fidelity compared to the direct simulation of the relaxation using the Kraus operators. However, this protocol requires no additional gates in the circuit which may give it an advantage as the system size grows and the implementation of the Kraus operators becomes increasingly complex. The causes and characteristics of the noise affecting the results must be understood better before the efficacy of scaling this protocol can be determined. Future work will address this issue.

V. ACKNOWLEDGMENTS

We thank Dr. V.A. Bagryansky (V.V. Voevodsky Institute of Chemical Kinetics and Combustion, Novosibirsk, Russia) for allowing use of his experimental data on quantum beats. This work was supported by the U.S. Department of Energy, Office of Science, Basic Energy Sciences, Division of Materials Sciences and Engineering under Grant No. de-sc0019469. B. R. was also supported by the National Science Foundation under Award DMR-1747426(QISE-NET). M. V. is supported by the IBM Global University Program. We acknowledge the use of IBM Q for this work. The views expressed are those of the authors and do not reflect the official policy or position of IBM or the IBM Q team.

¹ V. A. Bagryansky, V. I. Borovkov, and Y. N. Molin, Russian Chemical Reviews **76**, 493 (2007).

² Y. N. Molin, Mendelev Communications **14**, 85 (2004).

³ N. M. Yu, Bulletin of the Korean Chemical Society **20**, 7 (1999).

⁴ B. Brocklehurst, Chemical Society Reviews **31**, 301 (2002).

⁵ O. M. Usov, D. V. Stass, B. M. Tadjikov, and Y. N. Molin, The Journal of Physical Chemistry A **101**, 7711 (1997).

⁶ V. Bagryansky, O. Usov, N. Lukzen, and Y. N. Molin, Applied Magnetic Resonance **12**, 505 (1997).

⁷ M. Amy, D. Maslov, M. Mosca, and M. Roetteler, IEEE Transactions on Computer-Aided Design of Integrated Circuits and Systems **32**, 818 (2013).

⁸ 20-qubit backend: IBM Q team, “IBM Q 20 Almaden backend specification V1.3.1,” (2019).

- ⁹ V. Bagryansky, K. Ivanov, V. Borovkov, N. Lukzen, and Y. N. Molin, *The Journal of chemical physics* **122**, 224503 (2005).
- ¹⁰ Y. Molin and K. Salikhov, *Chemical Physics Letters* **211**, 484 (1993).
- ¹¹ J. Courtneidge, A. Davies, and D. McGucha, *Recueil des Travaux Chimiques des Pays-Bas* **107**, 190 (1988).
- ¹² M. M. Vyushkova, V. I. Borovkov, L. N. Shchegoleva, I. V. Beregovaya, V. A. Bagryansky, and Y. N. Molin, *Doklady Physical Chemistry* **420**, 125 (2008).
- ¹³ M. Vyushkova, P. Potashov, V. Borovkov, V. Bagryansky, and Y. Molin, in *Selectivity, Control and Fine Tuning in High-Energy Chemistry*, edited by D. V. Stass and V. I. Feldman (Research Signpost, Kerala, India, 2011) p. 191.
- ¹⁴ J. Preskill, "Lecture Notes for Physics 229: Quantum Information and Computation" (1998).
- ¹⁵ J. T. Barreiro, M. Müller, P. Schindler, D. Nigg, T. Monz, M. Chwalla, M. Hennrich, C. F. Roos, P. Zoller, and R. Blatt, *Nature* **470**, 486 EP (2011), article.
- ¹⁶ L. D. Re, B. Rost, A. F. Kemper, and J. K. Freericks, "Driven-dissipative quantum mechanics on a lattice: Describing a fermionic reservoir with the master equation and simulating it on a quantum computer," (2019), [arXiv:1912.08310 \[quant-ph\]](https://arxiv.org/abs/1912.08310).
- ¹⁷ H. Abraham, I. Y. Akhalwaya, G. Aleksandrowicz, T. Alexander, G. Alexandrowics, E. Arbel, A. Asfaw, C. Azaustre, P. Barkoutsos, G. Barron, L. Bello, Y. Ben-Haim, D. Bevenius, L. S. Bishop, S. Bosch, D. Bucher, CZ, F. Cabrera, P. Calpin, L. Capelluto, J. Carballo, G. Carrascal, A. Chen, C.-F. Chen, R. Chen, J. M. Chow, C. Claus, C. Clauss, A. J. Cross, A. W. Cross, J. Cruz-Benito, Cryoris, C. Culver, A. D. Córcoles-Gonzales, S. Dague, M. Dartiailh, A. R. Davila, D. Ding, E. Dumitrescu, K. Dumon, I. Duran, P. Eendebak, D. Egger, M. Everitt, P. M. Fernández, A. Frisch, A. Fuhrer, I. GOULD, J. Gacon, Gadi, B. G. Gago, J. M. Gambetta, L. Garcia, S. Garion, Gaweł-Kus, J. Gomez-Mosquera, S. de la Puente González, D. Greenberg, J. A. Gunnels, I. Haide, I. Hamamura, V. Havlicek, J. Hellmers, L. Herok, H. Horii, C. Howington, S. Hu, W. Hu, H. Imai, T. Imamichi, R. Iten, T. Itoko, A. Javadi-Abhari, Jessica, K. Johns, N. Kanazawa, A. Karazeev, P. Kassebaum, A. Kovyrshin, V. Krishnan, K. Krsulich, G. Kus, R. LaRose, R. Lambert, J. Latone, S. Lawrence, D. Liu, P. Liu, P. B. Z. Mac, Y. Maeng, A. Malyshev, J. Marecek, M. Marques, D. Mathews, A. Matsuo, D. T. McClure, C. McGarry, D. McKay, S. Meesala, A. Mezzacapo, R. Midha, Z. Mineev, M. D. Mooring, R. Morales, N. Moran, P. Murali, J. Müggenburg, D. Nadlinger, G. Nannicini, P. Nation, Y. Naveh, Nick-Singstock, P. Niroula, H. Norlen, L. J. O’Riordan, P. Ollitrault, S. Oud, D. Padilha, H. Paik, S. Perriello, A. Phan, M. Pistoia, A. Pozas-iKerstjens, V. Prutyantov, J. Pérez, Quintiii, R. Raymond, R. M.-C. Redondo, M. Reuter, D. M. Rodríguez, M. Ryu, M. Sandberg, N. Sathaye, B. Schmitt, C. Schnabel, T. L. Scholten, E. Schoute, I. F. Sertage, N. Shammah, Y. Shi, A. Silva, Y. Siraichi, S. Sivaramajah, J. A. Smolin, M. Soeken, D. Steenken, M. Stypulkoski, H. Takahashi, C. Taylor, P. Taylour, S. Thomas, M. Tillet, M. Tod, E. de la Torre, K. Trabing, M. Treinish, TrishaPe, W. Turner, Y. Vaknin, C. R. Valcarce, F. Varchon, D. Vogt-Lee, C. Vuillot, J. Weaver, R. Wieczorek, J. A. Wildstrom, R. Wille, E. Winston, J. J. Woehr, S. Woerner, R. Woo, C. J. Wood, R. Wood, S. Wood, J. Wootton, D. Yeralin, J. Yu, L. Zdanski, Zoufalc, anedumla, azulohner, bcamorrison, brandhsn, dennis-liu 1, drholmie, elfrocampeador, fanizamarco, gruu, kanejess, klinvill, lerongil, ma5x, merav aharoni, mrossinek, ordmoj, strickroman, tigerjack, yang.luh, and yotamvakninibm, "Qiskit: An open-source framework for quantum computing," (2019).